Two-dimensional phonon transport in supported graphene

Jae Hun Seol, Insun Jo, Arden L. Moore, Lucas Lindsay, Zachary H. Aitken, Michael T. Pettes, Xuesong Li, Zhen Yao, Rui Huang, David Broido, et al.

Two-Dimensional Phonon Transport in Supported Graphene

Jae Hun Seol,[1] Insun Jo,[2] Arden L. Moore,[1] Lucas Lindsay,[3,4] Zachary H. Aitken,[5] Michael T. Pettes,[1] Xuesong Li,[1,6] Zhen Yao,[2] Rui Huang,[5] David Broido,[3] Natalio Mingo,[7] Rodney S. Ruoff,[1,6] Li Shi[1,6]*

The reported thermal conductivity (κ) of suspended graphene, 3000 to 5000 watts per meter per kelvin, exceeds that of diamond and graphite. Thus, graphene can be useful in solving heat dissipation problems such as those in nanoelectronics. However, contact with a substrate could affect the thermal transport properties of graphene. Here, we show experimentally that κ of monolayer graphene exfoliated on a silicon dioxide support is still as high as about 600 watts per meter per kelvin near room temperature, exceeding those of metals such as copper. It is lower than that of suspended graphene because of phonons leaking across the graphene-support interface and strong interface-scattering of flexural modes, which make a large contribution to κ in suspended graphene according to a theoretical calculation.

Since graphene was first exfoliated from graphite and studied on dielectric substrates in 2004 (*1*), the monatomic layer of carbon atoms has attracted great interest for electronic applications because of superior charge mobility (*2*) and mechanical strength (*3*), as well as its compatibility with existing planar silicon devices. Other carbon allotropes, including diamond (*4*), graphite (*5*), and carbon nanotubes (CNTs) (*6*–*8*), have the highest thermal conductivity (κ) values reported because the strong bonding of the light carbon atoms results in a large phonon contribution to κ despite a much smaller electronic component. For similar reasons, graphene is

[1]Department of Mechanical Engineering, The University of Texas at Austin, Austin, TX 78712, USA. [2]Department of Physics, The University of Texas at Austin, Austin, TX 78712, USA. [3]Department of Physics, Boston College, Chestnut Hill, MA 02467, USA. [4]Department of Physics, Computer Science, and Engineering, Christopher Newport University, Newport News, VA 23606, USA. [5]Department of Aerospace Engineering and Engineering Mechanics, The University of Texas at Austin, Austin, TX 78712, USA. [6]Texas Materials Institute, The University of Texas at Austin, Austin, TX 78712, USA. [7]Laboratoire d'Innovation pour les Technologies des Energies Nouvelles et les Nanomatériaux, Commissariat à l'Énergie Atomique Grenoble, 17 rue des Martyrs, 38054 Grenoble, France.

*To whom correspondence should be addressed. E-mail: lishi@mail.utexas.edu

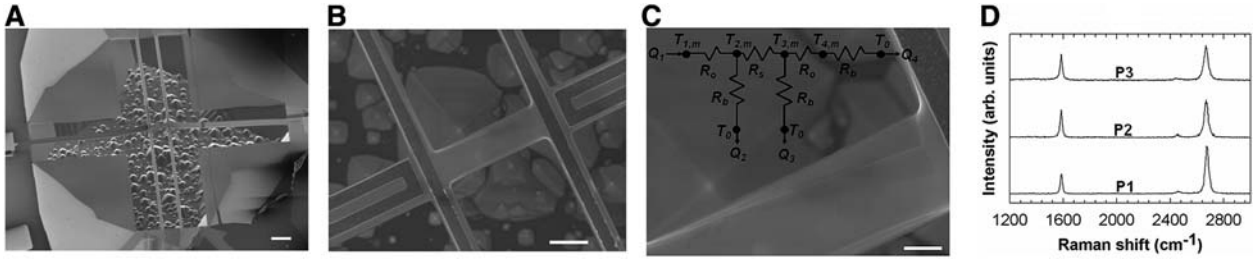

Fig. 1. Graphene sample G2. (**A** to **C**) SEM images of the suspended device, the central beam, and the folded edge of the SLG ribbon near the right electrode. The inset in (C) is a thermal circuit of the measurement device, where R_o is the thermal resistance of the SiO_2 joint between two adjacent RT lines. The scale bar is 10, 3, and 1 μm in (A), (B), and (C), respectively. (**D**) Raman spectra obtained from G2 immediately after the thermal measurement. The spectra (e.g., P1) obtained near the left end of the SLG indicates a monolayer sample, whereas those (such as P2 and P3) taken at the center and near the right electrode show a broadened 2D peak (centered at 2700 cm^{-1}) and a decreased 2D peak to G peak (centered at 1580 cm^{-1}) ratio because the folded-edge region of the SLG has a signal similar to that of bilayer graphene.

expected to possess a much higher κ than the silicon active layers and copper interconnects in current-generation electronic devices. This potential enhancement may provide a solution to the increasingly severe heat dissipation problem in nanoelectronics, which is caused by increased power density as well as reduced κ of electronic materials with decreasing feature sizes (*9*, *10*).

Although electronic transport in graphene has been investigated extensively, there have been few studies on the thermal transport because of experimental challenges. Recently, the room-temperature κ of a suspended single-layer graphene (SLG) flake has been reported from a Raman measurement (*11*). The obtained values, 3000 to 5000 W m^{-1} K^{-1}, exceed those of diamond (*4*) and graphite (*5*). However, because of the limited temperature (*T*) sensitivity of the Raman technique, this study has not yielded the $\kappa - T$ relation that is important for understanding the intriguing two-dimensional (2D) behavior of phonons in SLG. Furthermore, SLG is usually supported on a dielectric substrate for device applications. The charge mobility in SLG supported on silicon dioxide (SiO_2) is suppressed by about 10 times compared with clean suspended SLG because of scattering by substrate phonons and impurities (*12*). The effect of substrate interaction on thermal transport, however, has not been elucidated so far.

Here, we report thermal transport measurements on SLG supported on amorphous SiO_2, which represents the most commonly used device configuration. Despite phonon-substrate scattering, we find that the room-temperature κ of the supported SLG approaches about 600 W m^{-1} K^{-1}, considerably higher than the κ values of common thin-film electronic materials (*9*, *10*). In addition, using full quantum mechanical calculations of the three-phonon scattering processes, we find a large κ contribution from the flexural (ZA) modes in suspended SLG. The measured $\kappa - T$ relation can be explained by large suppression of the ZA contribution in the supported SLG.

We made thermal measurements on three SLG flakes exfoliated onto SiO_2 using the device shown in Fig. 1, A to C (*13*). The patterned SLG of 1.5 to 3.2 μm in width (*W*) and 9.5 to 12.5 μm in length (*L*) covers the surface of a ~300-nm-thick SiO_2 beam, the two ends of which are connected to four Au/Cr resistance thermometer (RT) lines on suspended SiO_2 beams. The two straight inner RT lines cover the two ends of the SLG, which does not contact the two outer U-shaped RT lines.

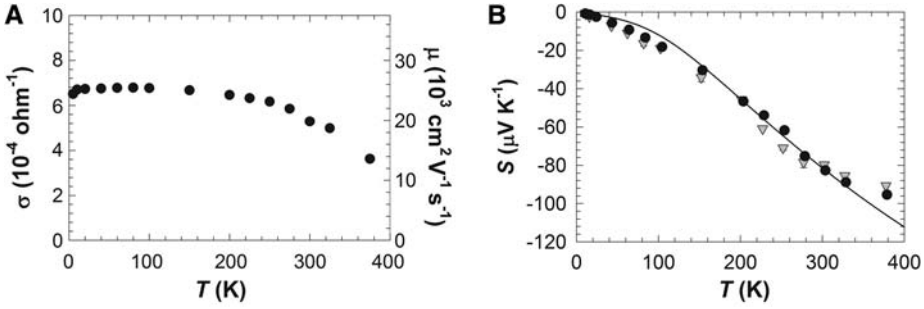

Fig. 2. (**A**) Measured two-probe electrical conductivity (σ) and extracted electron mobility (μ) of G2 as a function of temperature. (**B**) Measured Seebeck coefficients as a function of temperature for G1 (triangles) and G2 (circles). The error bars reported in this work include both bias and random uncertainties, the latter of which are determined based on three to nine measurements.

The SLG samples were characterized with Raman spectroscopy and scanning electron microscopy (SEM) (*13*). Sample 1 (G1) consists of a 3.2-μm-wide ribbon and a 1.5-μm-wide ribbon in parallel. Although a portion of one edge of the 2.4-μm-wide sample 2 (G2) is folded near one electrode (Fig. 1C), the two edges of the 2.4-μm-wide sample 3 (G3) appear to be straight. In addition, the obtained Raman spectra show that G1, G2 (Fig. 1D), and G3 are monolayers with no indication of the D band associated with defects (*14*).

The two-probe electrical resistance (*R*) at room temperature was measured to be 160, 7, and 5400 kilohm for G1, G2, and G3, respectively. The much lower two-probe *R* of G2 is indicative of smaller contact resistance and a cleaner electrode-graphene interface than for the other two samples. For G2 (Fig. 2A), the two-probe, 2D electrical conductivity, $\sigma \equiv L/WR$, shows a *T* dependence similar to that reported for oxide-supported SLG (*12*).

We measured the Seebeck coefficient (*S*) of the SLG by electrically heating one outer U-shaped RT line (RT 1). Because of a linear temperature profile between the midpoint and the ends of the other three RT lines (RT 2, 3, and 4 in order of increasing distance from RT 1, respectively), the highest temperature rise at the midpoint ($\Delta T_{j,m}$) is twice the average rise ($\overline{\Delta T_j}$) of each of the three lines (*13*), i.e., $\Delta T_{j,m} \equiv T_{j,m} - T_0 = 2\overline{\Delta T_j}; j = 2,3,4$, where T_0 is the substrate temperature. Using the thermal circuit in Fig. 1C and averaging the parabolic temperature profile of RT 1, we derive (*13*)

$$\Delta T_{1,m} = \frac{3}{2}\overline{\Delta T_1} - \frac{1}{2}(\overline{\Delta T_2} + \overline{\Delta T_3} + \overline{\Delta T_4}) \quad (1)$$

where $\overline{\Delta T_j}$ is obtained from the measured four-probe electrical resistance of each RT line. The measurement yields $S = V_{23}/(\Delta T_{2,m} - \Delta T_{3,m})$, where V_{23} is the thermovoltage between the two inner electrodes.

The obtained room-temperature *S* values of G1 and G2 (Fig. 2B) are –79.7 ± 0.6 and –82.7 ± 0.2 μV K^{-1}, respectively, which suggests that the Fermi energy (E_F) is in the conduction band. We fit the experimental $S-T$ curve using a theoretical model (*15*) for oxide-supported SLG where screened charged impurity scattering dominates electron transport. For G2, the best fit to the measured *S* is given by $E_F = 0.049$ eV (*13*). The electron concentration is obtained as $n = (E_F/\hbar v_F)^2/\pi = 1.7 \times 10^{11}$ cm^{-2}, where $\hbar$ is the reduced Planck's constant, and $v_F = 1 \times 10^6$ m/s is the Fermi velocity in SLG. Based on $\mu = \sigma/ne$, with *e* being the elemental charge, a μ value of

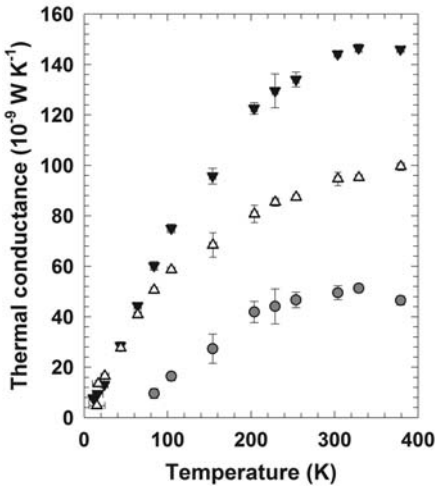

Fig. 3. Measured thermal conductance of G2 before (solid downward triangles) and after (unfilled upward triangles) the SLG was etched, with the difference being the contribution from the SLG (circles).

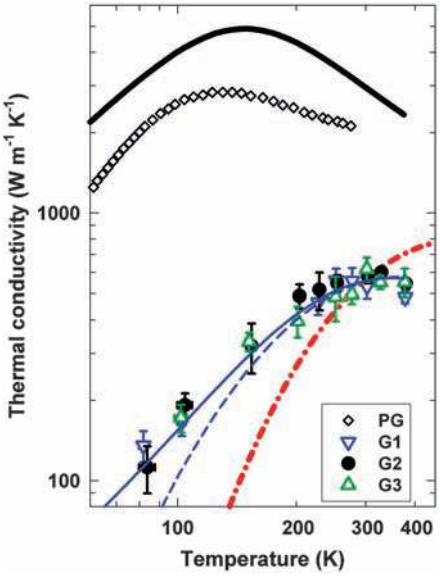

Fig. 4. Measured thermal conductivity of G1, G2, and G3 together with the highest reported values of PG (*5*), the BTE calculation results of suspended SLG (black solid line) and supported SLG with $K_{LATA} = 0$ and $K_{ZA} = 0.73$ N/m (blue solid line) or $K_{LATA} = K_{ZA} = 0.46$ N/m (blue dashed line), the RTA calculation result (red dashed-dotted line) for supported SLG with $K_{LATA} = 0.8$ N/m. Specular edges are assumed in the calculations. For supported SLG, $s = d = 30$ nm, and the calculation results are insensitive to edge specularity and can be reproduced with decreased d/s and increased K_{ZA} for the same K_{LATA}/K_{ZA}.

~20,000 cm^2/Vs (Fig. 2A) is obtained, comparable to the highest electron mobility values reported for oxide-supported SLG (*12*, *16*), thus suggesting similar sample quality.

For the κ measurement, the thermal resistance of each RT line including the SiO_2 beam is the same and was obtained as (*13*)

$$R_b = 2\frac{\Delta T_{1,m} + \Delta T_{2,m} + \Delta T_{3,m} + \Delta T_{4,m}}{Q} \quad (2)$$

where Q is the electrical heating in RT 1. The thermal resistance of the central beam is found from the thermal circuit as

$$R_s = R_b \frac{\Delta T_{2,m} - \Delta T_{3,m}}{\Delta T_{3,m} + \Delta T_{4,m}} \quad (3)$$

and was several orders of magnitude higher than the calculated interface thermal resistance between the SLG and the electrode or the SiO_2 (*13*). The thermal conductance ($G \equiv 1/R_s$) of the central beam was measured before and after the SLG was etched away in oxygen plasma. The measured G after etching was considerably smaller than that before etching for T above 80 K, below which the difference decreases to near the measurement uncertainty (Fig. 3). The difference in G before and after the etching is attributed to the thermal conductance of the SLG, G_g. We follow the convention to obtain $\kappa = G_g L/Wt$, where we use the interlayer spacing in graphite as the SLG thickness, $t = 0.335$ nm. The results are similar for the three samples (Fig. 4). For G2, the room-temperature κ of 579 ± 34 W m^{-1} K^{-1} is about a factor of 3.4 lower than the highest reported basal-plane value of pyrolytic graphite (PG) (*5*). The appearance of the peak κ position at a much higher $T \approx 300$ K in the supported SLG than $T \approx 140$ K in the PG suggests that phonon scattering is dominated by substrate interaction and umklapp scattering at below and above 300 K, respectively.

Interestingly, Klemens (*17*) had envisioned the feasibility of our thermal measurements several years before SLG was first exfoliated onto SiO_2 (*1*). He suggested that phonons leaking from supported SLG into the substrate would suppress the contribution of low-frequency phonons and reduce κ by 20 to 50%. In SLG, the longitudinal (LA) and in-plane transverse (TA) acoustic branches are linear, whereas the out-of-plane ZA branch shows a quadratic dependence of the frequency (ω) on the wave vector. The contribution to κ from the ZA branch would be negligible based on a relaxation time approximation (RTA) model (*18*) because of the small group velocity and large umklapp scattering rate (τ_u^{-1}) calculated from an expression derived by Klemens and Pedraza (*19*).

In addition to a long wavelength approximation and the assumptions of a linear branch and high T, Klemens and Pedraza cautioned that the greatest uncertainty in their τ_u^{-1} expression stems from the inaccuracy of the assumed three-phonon scattering phase space that was not explicitly calculated (*19*). To address this problem, we carried out full quantum mechanical calculations of both normal and umklapp three-phonon scattering processes in SLG throughout the Brillouin zone (*13*). Through the calculations of the three-phonon matrix elements, we obtain a selection rule for three-phonon scattering, which requires that an even number of ZA phonons be involved in each process as a consequence of the reflection symmetry in flat 2D SLG (*13*). We note that this selection rule was not used in a recent calculation (*20*), whereas an analogous selection rule has been found for electron-ZA phonon scattering in SLG (*21*). This selection rule strongly restricts the phase space for umklapp scattering of ZA phonons in flat SLG. We also find that this selection rule applies in large-radius single-walled CNTs whose curvature is comparable to that of ripples that can form in SLG. We have incorporated this selection rule in an exact numerical solution of the linearized phonon Boltzmann transport equation (BTE) for SLG. Our BTE approach is similar to that used recently for nanotubes (*22*). We find that the ZA modes can contribute as much as 77% and 86% of the total calculated κ at 300 K and 100 K, respectively, for a 10-μm-long suspended SLG with specular edges and 1.1% C^{13} isotopic impurities (*13*). The calculated κ for the suspended SLG is about a factor of 5 and 1.5 higher than the measured κ of the supported SLG and the PG, respectively, at $T \approx 300$ K (Fig. 4).

Scanning probe microscopy measurements have found that SLG exfoliated on SiO_2 is partially conformal to the surface roughness (*23*) and partly suspended between hills on the surface (*24*). These experiments consistently obtained a substrate-induced correlation length in SLG of ~30 nm, which gives a measure of the average center-to-center separation (s) between adjacent hills in intimate contact with the SLG. Perturbation theory yields an approximate expression for the scattering rate due to phonon leakage back and forth across the contact patches as $\tau_{sub,j}^{-1} \propto \rho_j(\omega) K_j^2/\omega^2$, where $\rho_j(\omega)$ depends on the phonon density of states, and K_j is the average van der Waals (vdW) interatomic force constant between the SLG and the SiO_2 support for polarization j = ZA, TA, or LA (*13*). A similar frequency dependence has been obtained for phonon transmission across a vdW interface between two half spaces (*25*). In our case, the expression accounts for parallel momentum not being conserved due to the amorphous structure of the SiO_2 support. The obtained $\tau_{sub,j}^{-1}$ increases with the diameter (d) of the contact patches and the d to s ratio (*13*).

Based on the interlayer vdW energy $\Gamma_0 \approx 0.1$ J/m^2 in graphite and the measured average SLG-SiO_2 separation $h_0 \approx 0.42$ nm reported in (*23*), we calculate $K_{ZA} = 27 S_a \Gamma_0 / h_0^2 \approx 0.4$ N/m, where S_a is the area occupied by one carbon atom in graphene (*13*). The interface force constant K_{LATA} for the in-plane LA and TA modes is generally smaller than K_{ZA} (*26*), especially for an amorphous substrate. At the upper limit of $K_{LATA} = K_{ZA} = 0.46$ N/m and $d = s = 30$ nm, the BTE model obtains a κ value close to the measured value at 300 K, and yields a large ZA contribution (*13*). However, the calculated κ increases

with T at a steeper rate than the measurement result (Fig. 4). In comparison, at the lower limit of $K_{LATA} = 0$, $K_{ZA} = 0.73$ N/m, and $s = d = 30$ nm, the BTE solution obtains a $\kappa - T$ curve in good agreement with the measurement (Fig. 4). In this case, the ZA contribution to κ becomes smaller than the corresponding TA and LA contributions (*13*), which are reduced only by the suppression of the ZA + ZA → LA or TA mode conversions because of leakage of ZA phonons.

In 2D and at the low T limit, if the scattering rate τ_j^{-1} is proportional to ω^{α}, the κ contribution is proportional to $T^{2-\alpha}$ for j = TA, LA, or ZA polarization. For $K_{LATA} = K_{ZA} = 0.46$ N/m, τ_j^{-1} of all the three polarizations is dominated by $\tau_{sub,j}^{-1}$, for which the α exponent is negative and results in an increased κ with T. In comparison, for $K_{LATA} = 0$ and $K_{ZA} = 0.73$ N/m, boundary scattering with $\alpha = 0$ and isotope and umklapp scatterings with positive α exponents play an increased role for the dominant in-plane polarizations at low and intermediate T, respectively, so that the calculated $\kappa - T$ slope in this T range is relatively small, in agreement with the measured data. On the other hand, we have also fit the measured κ at 300 K by including substrate scattering of $K_{LATA} = 0.8$ N/m in the RTA model (*18*) that neglects the ZA contribution (*13*). The as-calculated κ increases with T at a much more rapid rate than both the BTE results and the experimental data (Fig. 4), because of the negative α exponent of the dominant substrate scattering rate for the LA and TA phonons and the high zone-boundary frequencies of these two branches.

The theoretical analysis suggests that the ZA contribution to κ is large in suspended SLG and that the measured $\kappa - T$ relation can be explained by much stronger substrate scattering of ZA phonons than LA and TA phonons. Although the strong ZA scattering can be caused by the expected behavior of $K_{ZA} > K_{LATA}$, another possibility is that umklapp scattering of ZA phonons can be enhanced by the substrate interaction, which breaks the reflection symmetry. Indeed, our calculations show that the ZA contribution is reduced in suspended bilayer graphene because of interlayer interactions. Although future theoretical work is needed to clarify this issue, our experimental results clearly show that graphene exfoliated on SiO_2 still conducts heat rather efficiently despite phonon-substrate interaction. However, the substrate effect could be quite different for few-layer graphene or SLG grown by thermal decomposition (*27*) or chemical vapor deposition (*28*, *29*) on other substrates because of different interface interactions. These intriguing questions are expected to stimulate further experimental and theoretical investigations of phonon transport in suspended, supported, and embedded graphene.

References and Notes

1. K. S. Novoselov *et al*., *Science* **306**, 666 (2004).
2. K. I. Bolotin *et al*., *Solid State Commun.* **146**, 351 (2008).
3. C. Lee, X. Wei, J. W. Kysar, J. Hone, *Science* **321**, 385 (2008).
4. G. A. Slack, *J. Appl. Phys.* **35**, 3460 (1964).
5. G. A. Slack, *Phys. Rev.* **127**, 694 (1962).
6. P. Kim, L. Shi, A. Majumdar, P. L. McEuen, *Phys. Rev. Lett.* **87**, 215502 (2001).
7. C. Yu, L. Shi, Z. Yao, D. Li, A. Majumdar, *Nano Lett.* **5**, 1842 (2005).
8. E. Pop *et al*., *Phys. Rev. Lett.* **95**, 155505 (2005).
9. Y. S. Ju, K. E. Goodson, *Appl. Phys. Lett.* **74**, 3005 (1999).
10. Y. Yang, W. Liu, M. Asheghi, *Appl. Phys. Lett.* **84**, 3121 (2004).
11. A. A. Balandin *et al*., *Nano Lett.* **8**, 902 (2008).
12. J. H. Chen, C. Jang, S. Xiao, M. Ishigami, M. S. Fuhrer, *Nat. Nanotechnol.* **3**, 206 (2008).
13. Materials and methods are available as supporting materials on *Science* Online.
14. L. M. Malard, M. A. Pimenta, G. Dresselhaus, M. S. Dresselhaus, *Phys. Rep.* **473**, 51 (2009).
15. E. H. Hwang, E. Rossi, S. Das Sarma, *Phys. Rev. B* **80**, 235415 (2009).
16. Y.-W. Tan *et al*., *Phys. Rev. Lett.* **99**, 246803 (2007).
17. P. G. Klemens, *Int. J. Thermophys.* **22**, 265 (2001).
18. D. L. Nika, S. Ghosh, E. P. Pokatilov, A. A. Balandin, *Appl. Phys. Lett.* **94**, 203103 (2009).
19. P. G. Klemens, D. F. Pedraza, *Carbon* **32**, 735 (1994).
20. D. L. Nika, E. P. Pokatilov, A. S. Askerov, A. A. Balandin, *Phys. Rev. B* **79**, 155413 (2009).
21. E. Mariani, F. von Oppen, *Phys. Rev. Lett.* **100**, 076801 (2008).
22. L. Lindsay, D. A. Broido, N. Mingo, *Phys. Rev. B* **80**, 125407 (2009).
23. M. Ishigami, J. H. Chen, W. G. Cullen, M. S. Fuhrer, E. D. Williams, *Nano Lett.* **7**, 1643 (2007).
24. V. Geringer *et al*., *Phys. Rev. Lett.* **102**, 076102 (2009).
25. R. Prasher, *Appl. Phys. Lett.* **94**, 041905 (2009).
26. M. T. Dove, *Introduction to Lattice Dynamics, Cambridge Topics in Mineral Physics and Chemistry 4* (Cambridge Univ. Press, Cambridge, New York, 1993), pp. 29–32.
27. C. Berger *et al*., *J. Phys. Chem. B* **108**, 19912 (2004).
28. K. S. Kim *et al*., *Nature* **457**, 706 (2009).
29. X. Li *et al*., *Science* **324**, 1312 (2009).

30. This work is supported in part by National Science Foundation awards CBET-0553649 and 0933454 (J.H.S. and L.S.), CBET 0651381 (D.A.B. and L.L.), 0651310 (N.M.), and CMMI-0926851 (Z.H.A. and R.H.); Office of Naval Research award N00014-08-1-1168 (A.L.M. and L.S.); Department of Energy Office of Science award DE-FG02-07ER46377(M.T.P. and L.S.); and The University of Texas at Austin (R.S.R.).